Design and Simulation of a Highly Discriminant Laser Array Waveguide

by

Jennifer Anne Healey

Submitted to the Department of Electrical Engineering and Computer Science
in partial fulfillment of the requirements for the degree of

Master of Science in Computer Science and Engineering

at the

MASSACHUSETTS INSTITUTE OF TECHNOLOGY

December 1994

Author .....
Department of Electrical Engineering and Computer Science
December 1, 1994

Certified by .....
Hermann A. Haus
MIT Professor
Thesis Supervisor

Certified by .....
Karl M. Kissa
Technical Supervisor, Draper Laboratory
Thesis Supervisor

Accepted by .....
F. R. Morgenthaler
Chair, Departmental Committee on Graduate Students

Design and Simulation of a Highly Discriminant Laser Array Waveguide

by

Jennifer Anne Healey

Submitted to the Department of Electrical Engineering and Computer Science
on December 1, 1994, in partial fulfillment of the
requirements for the degree of
Master of Science in Computer Science and Engineering

Abstract

The laser array waveguide designed and simulated in this thesis is highly mode discriminant and able to take advantage of spatially dispersive high-power pumping sources, such as, semiconductor laser diode arrays. The waveguide measures 5cm $\times$ 0.5cm and consists of an array of five $4\mu m \times 4\mu m$ single mode Nd^{+3} doped glass lasers embedded in double cladding to improve total pumping efficiency. The gain profile of the array is designed so that the device lases only in the fundamental supermode; regardless of the mode of the pump source or of minor deviations from exact parallelism at the end faces. A simulation of the performance of the device was conducted with a the Beam-Propagation Method. Results of the simulation indicated that a coherent phase-locked beam is always produced from this laser waveguide array.

Thesis Supervisor: Hermann A. Haus
Title: MIT Professor

Thesis Supervisor: Karl M. Kissa
Title: Technical Supervisor, Draper Laboratory

Acknowledgments

I would like to thank Prof. Haus for his valued criticism and guidance which directed the research of this thesis. I would like to thank Karl Kissa for his constant supervision, encouragement and guidance throughout the project and also for the design and development of computer software which made this analysis possible. Furthermore, I would like to thank Jerry Chen for his knowledge of Project Athena, Makefiles and the C programming language and Rick Tumminelli for developing the double-clad structure and for finding the funding for this project.

Contents

List of Figures

List of Tables

Chapter 1

Introduction

The laser array waveguide that has been designed and simulated in this thesis is highly mode discriminant and provides one of the best ways to take advantage of the high power of low cost semiconductor laser diode arrays. If semiconductor arrays could be mode-locked to lase in the fundamental supermode, they would provide an ideal high-power, low-cost, compact, coherent laser beam. However, internal conduction in semi-conductors creates very poor discrimination for the supermodes of laser arrays and prohibits mode-locking the device in the fundamental supermode. Therefore, semiconductor laser diode arrays can lase only in higher order spatial modes, which are unable to produce a coherent beam and are thus unable to be focused to a point.

Many attempts have been made to harness the power of the semi-conductor laser array into a coherent beam. Most attempts have used external mode control mechanisms to lock the array into the fundamental mode [1]. Some successful methods include injection mode-locking from a second laser [2] and the use of external bulk optics such as tunable grating cavities [3], photo-refractive phase conjugate mirrors [4] and corner reflectors [5].

The basic design of the laser array presented here is shown in Figure 1-1. It is an improvement over these other methods because it is extremely compact and sturdy. The glass waveguide is end-butt coupled to the semiconductor laser array as shown in Figure 2-1 making the entire area of the structure only 6cm $\times$ .5cm. This coupling arrangement is far less sensitive to misalignment than endfire coupling because of the high numerical aperture and large coupling area of the inner cladding. It can stand misalignment of $\pm 1\mu$ vertically and $\pm 5\mu$ horizontally and still maintain lasing activity. The glass waveguide can use the multi-mode output of the semiconductor laser diode array because it is optically rather than electrically pumped. This allows it to have high mode discrimination because the modes are confined by total internal reflection rather than electrical potentials which suffer losses due to defects in the regions between the guides.

The laser array consists of five laser ribs of doped with a rare earth element, surrounded with

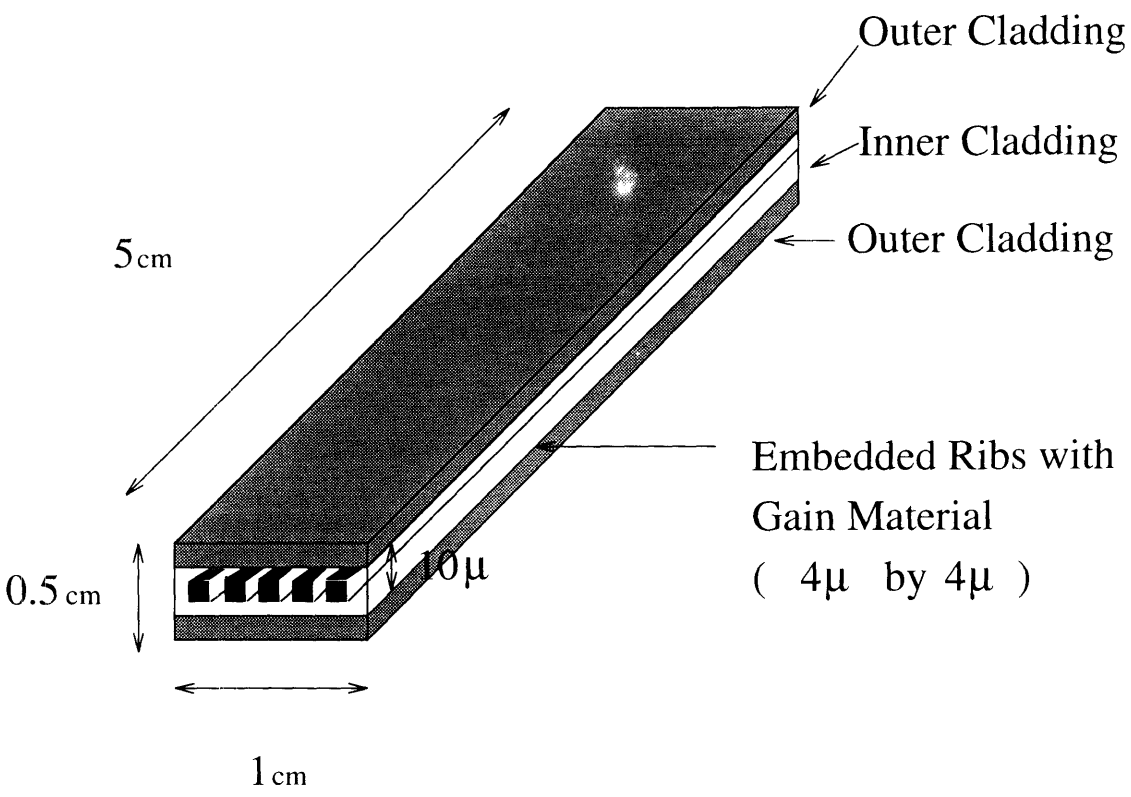

Figure 1-1: A Simplified Diagram of the Waveguide

a double cladding. The double cladding surrounds the laser ribs as shown in Figure 2-2. Forty percent of the light from the diode array is trapped by the inner cladding of the waveguide. Some of this light will couple directly into the lasers; however, most of it will be absorbed indirectly as it passes through the lasers and down the inner cladding. When enough energy has been absorbed the population inversion increases to its threshold value and lasing occurs. If the gain profile is properly selected, fundamental supermode of the array will dominate the array and all the individual lasers will be locked in phase with each other. The gain profile is selected by controlling the doping the ribs and creating reflection losses at the pump wavelength.

Extensive computer modeling was used to test the feasibility of the design. The five laser waveguide was modeled and analyzed with a finite-difference beam-propagation method (BPM). BPM calculates the time-independent solution to Maxwell's equations at designated steps throughout the waveguide. To check the accuracy of this computer simulation, we simulated a slab waveguide, for which the analytic solution is known and compared the field predicted by analytic methods with the output electric field generated by the BPM simulation. A very good correspondence was shown as discussed in Section 3.3.

A matrix array program was used to determine the laser spacings and gain profile for the BPM model. This program reduced the three dimensional waveguide to a two dimensional multi-layer stack

using an effective index method and found the gain per centimeter of the supermodes of the array. Although this program was not necessary to prove the validity of this thesis, it was able to determine the dominant supermode over one hundred times faster than a BPM simulation. Therefore it was used extensively to experiment with various designs for the gain profile. When a feasible gain profile was found, it was modeled and simulated with the BPM program. The BPM program calculated the output fields and found that the array would lase in the fundamental supermode and would create a coherent output beam.

Once a working design had been established, fabrication issues were considered. The practical implementation of the gain profile, the device's tolerance to deviations in end-face parallelism and pumping devices of different spatial modes were investigated. It was found that a non-uniform doping profile was difficult to achieve, because all the lasers would be fabricated in a single melt. A simpler solution was to regulate the gain profile through reflection losses at the pump wavelength. End face parallelism tolerance was tested by adding a linearly increasing phase delay, proportional to the angle of deviation, to the electric field at one end of the waveguide. Tolerances up to the maximum error for Draper Laboratory's manufacturing capabilities (one arc-second) were tested. No effect on device performance was found. Finally, the device's sensitivity to the initial spatial mode of the array was tested. The initial condition of the BPM simulation was varied to verify that the fundamental supermode was dominant. It was found that the device would lase in the fundamental mode even in the most adverse conditions when the initial field was chosen to be very similar to an orthogonal higher order supermode.

Chapter 2

The Design of the Physical Device

2.1 Pumping with a Double Cladding

The waveguide modeled in this simulation was pumped by a laser diode array butt-coupled to the guide as shown in Figure 2-1. The light from the pump is captured by the double cladding structure shown in Figure 2-2. In most fiber lasers, the lasing material is pumped directly through end-fire pumping. Although this method is very efficient, it requires careful alignment ($\pm 0.1\mu$) of the pump beam and the end of the laser. The endbutt coupling is far more tolerant to misalignment ($\pm 1\mu$ vertically and $\pm 5\mu$ horizontally), but it is so inefficient that without the double cladding, less than 5% of the pump light could be captured by the ribs. The double cladding design allows the waveguide to be butt-coupled to the laser diode array because the inner cladding will capture a large percentage of the pump light.

In the typical single cladding design, only a small amount of light would end-fire directly into the ribs and be captured for lasing. As it propagated, this light would be absorbed by the gain material according the the absorption equation:

$$P(x) = P_o e^{-2\alpha_n x} \tag{2.1}$$

where $P(x)$ is the power at point x, P_o is the initial power and α_n is the absorption coefficient for the dopant rare earth ion. The light which is not captured by the rib simply radiates away without pumping the laser.

To capture more power from the laser diode array, a double cladding was proposed. In this structure, shown in Figure 2-2, a higher indexed inner cladding (n_i) surrounds the laser ribs (n_r) where $n_r > n_i > n_o$. The percentage of captured light is determined by the ratio the numerical

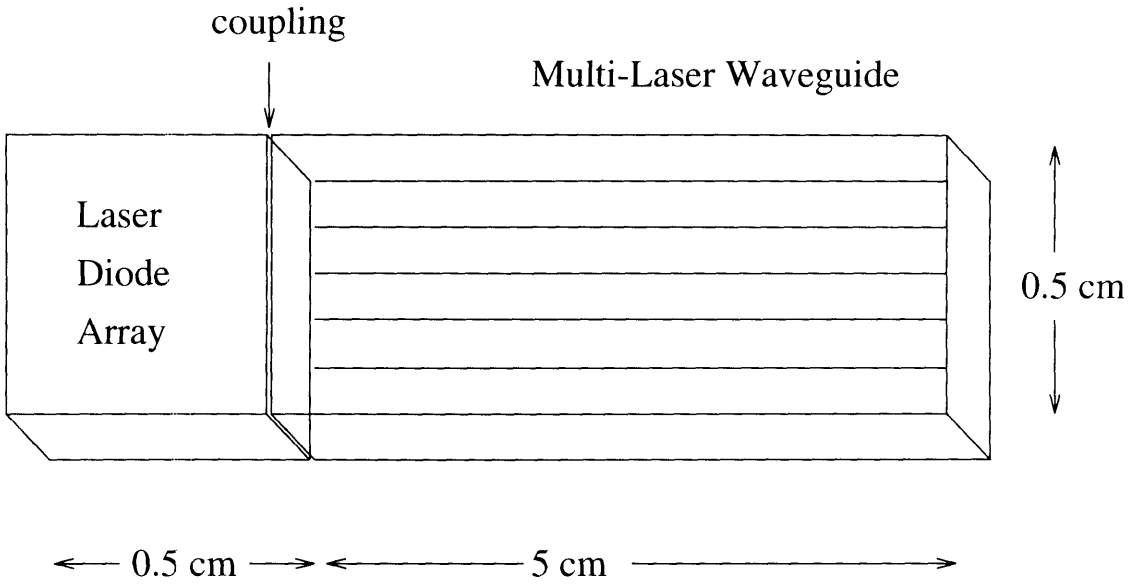

Figure 2-1: A Diagram of an Endbutt Configuration

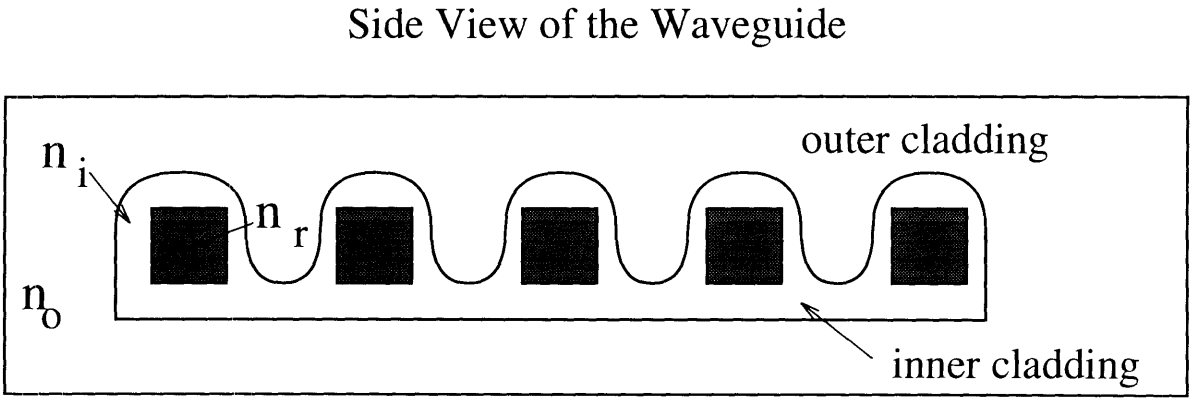

Figure 2-2: A Diagram of the Double Cladding

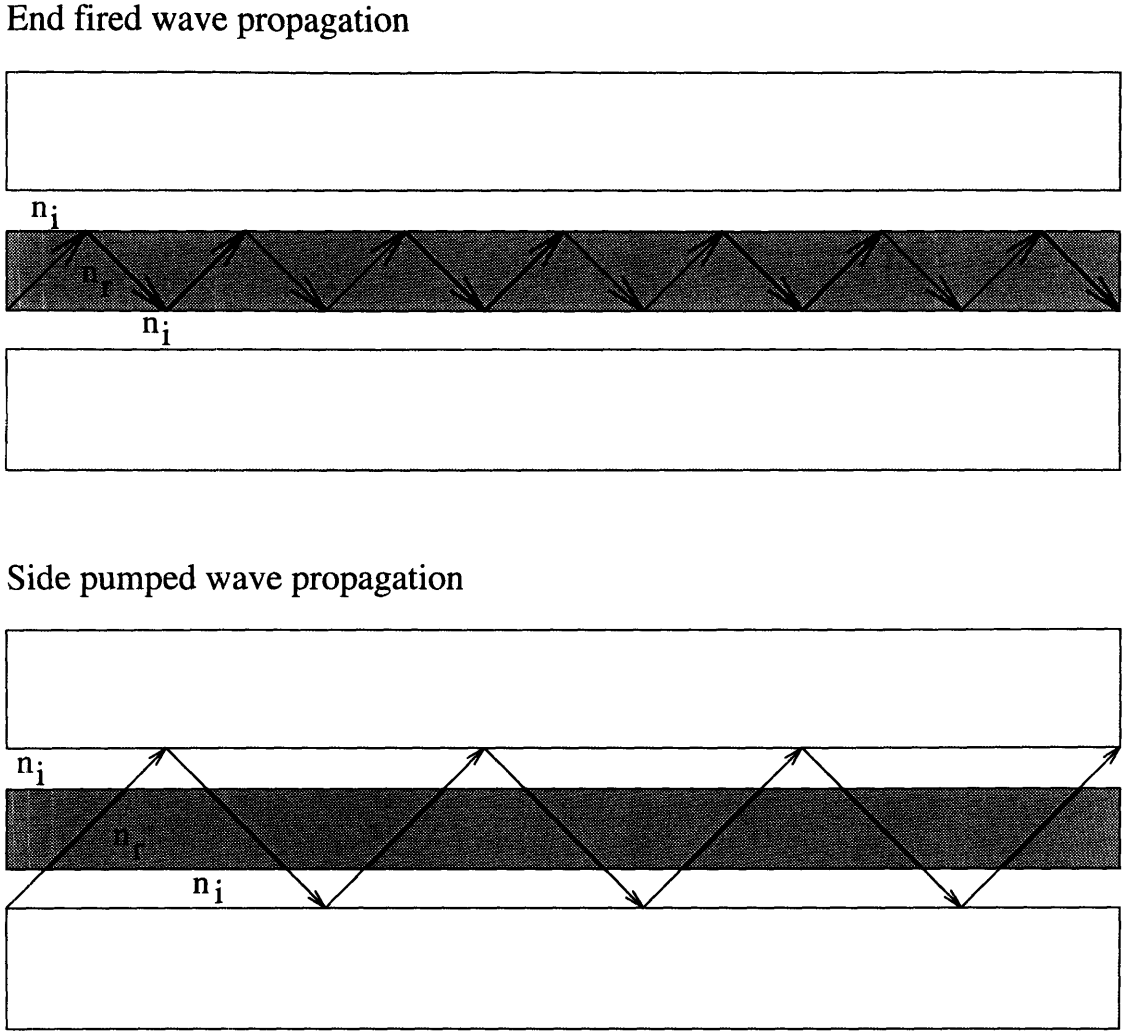

Figure 2-3: The Propagation of Light through the Gain Medium

aperture (N. A.) which depends of the differences in the indices:

$$N.A. = \sqrt{n_i^2 - n_o^2} \tag{2.2}$$

In this design we use a model with $n_i = 1.49$ and $n_o = 1.45$, the maximum index difference allowed by the fabrication process. This design allows 34% of the light emitted by the source to be captured by the inner cladding. Only approximately one-fifth of the 34% couples directly into the laser ribs. If there were no inner cladding, the rest of the light would radiate away without pumping the laser. With the inner cladding, the remaining light captured is absorbed by the lasers when it crosses through the gain material as it propagates down the waveguide.

Figure 2-3 is a simplified diagram of how the light in the inner cladding crosses through the gain medium where it can be absorbed. This diagram shows that light which is not end-fired directly

is less absorbed than light which is end-fired, however, it is difficult to determine analytically the fraction of light absorbed, per pass, through the rib. This difficulty arises because the light captured by the inner cladding is highly multi-mode, both horizontally and vertically. Every mode has a different overlap integral with the laser ribs and the relative strengths of the modes is not known. To calculate the fill factor of the absorbing material accurately, the overlap integrals of all the modes would have to be determined and weighted by the relative strength of their mode. The fill factor would be the weighted sum of these modes. This calculation would be too difficult to perform analytically, therefore a BPM simulation was used to estimate how quickly the power from the laser diode array. The laser ribs were modeled as a slab waveguide with the BPM program to find the fill

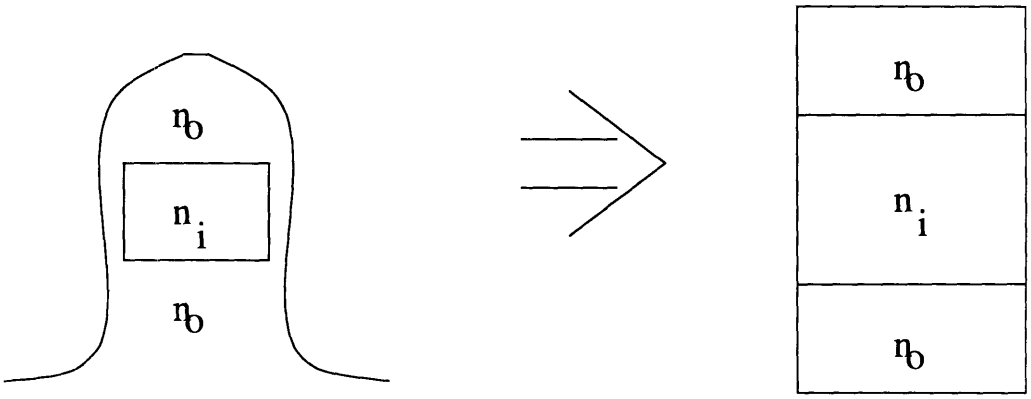

Figure 2-4: The Model for the Fill Factor

factor (See Figure 2-4). The BPM program used a bulk absorption value of $3.3\frac{dB}{cm}$ for the material in the ribs (a typical value for Neodymium) and calculated the intensity of the field as the pump light propagated down the waveguide. The intensity of the pump light was sampled every 10 microns. The positions and the intensities were entered into an EXCEL^{TM} spreadsheet. The rate of absorption in $\frac{dB}{cm}$ was calculated using the equation:

$$\alpha_n(\frac{dB}{cm}) = \frac{10log\frac{P}{P_o}}{x(cm)} \tag{2.3}$$

It was determined by this method that total absorption of all pump light captured by the inner cladding was 1.2 $\frac{dB}{cm}$. This value indicates that 75% of the pump light will be absorbed at 5cm, before the first reflection and 94% of the pump light will be absorbed at 10cm propagation, before the second reflection. Therefore, the estimated 2% loss at the mirrors will only result in an insignificant power loss of less than 1%.

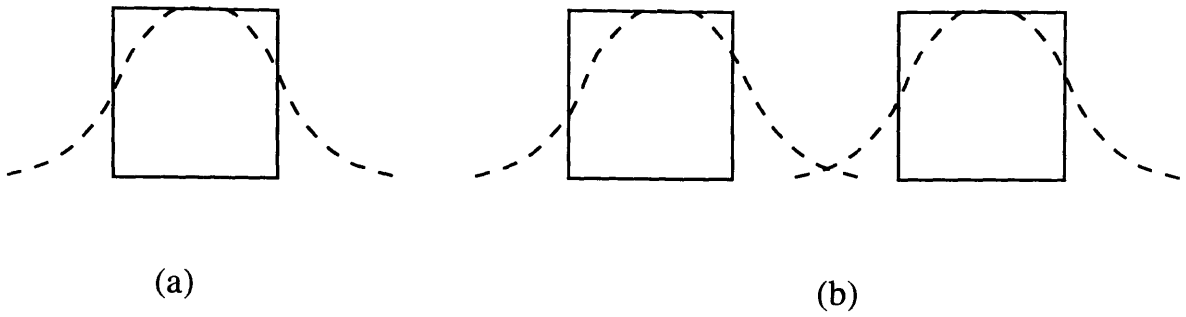

Figure 2-5: The Mode Distribution in a Single Mode Rib

2.2 Modelocking in the Fundamental Supermode

As the lasers absorb power through a combination of direct and indirect pumping, the population inversion between the upper and lower lasing levels increases until a threshold value is reached. At threshold, each of the $4\mu m \times 4\mu m$ ribs begins to lase individually. The transverse dimensions of the laser ribs are small enough to insure that each rib supports only the fundamental transverse mode. This mode has the shape of a gaussian distribution as shown in Figure 2-5(a). The mode has evanescent tails which extend into the inner cladding. When two ribs are placed close enough together, the evanescent tails of their modes overlap. This overlap allows the ribs to communicate with each other and influence the phase of the lasing with respect to each other. This influence can produce a supermode of the array. If the lasers all lase with equal strength, the highest order supermode, shown in Figure 2-6, will dominate the structure and the lasers will lase 180° out of phase with their nearest neighbors. By changing the strength of the lasers, different supermodes dominate the structure. Lasing strength can be adjusted by either doping the ribs with fewer rare earth ions or by creating lossy mirrors at the ends of the ribs.

The relationship between the gain in the lasers and the dominant supermode can be seen in Figure 2-7 (a). The peaks and dips of the five modes correspond to the placement of the laser ribs as shown in Figure 2-7 (b). To promote the fundamental supermode, gain was placed only in the region indicated by the dotted rectangle in Figure 2-7 (b). In this region, the fundamental mode had the greatest peaks. In the region outside the rectangle the fundamental mode has the smallest intensity, and would benefit the least from gain. Through experimentation a matrix mode solver (discussed in Section 3.4), it was found that it was necessary to dope both the inner cladding and the ribs to strongly promote the fundamental mode. Doping the inner cladding creates a solid region of gain in the middle section of the waveguide which allows the fundamental mode to take advantage of gain where the other modes have nodes. An imaginary index of 2.47×10^{-5} per micron was used to model the gain. This value was taken from experiments with double clad fibers doped with one weight percent Neodymium.

The region outside the dotted rectangle was modeled as having no gain. In a physical device,

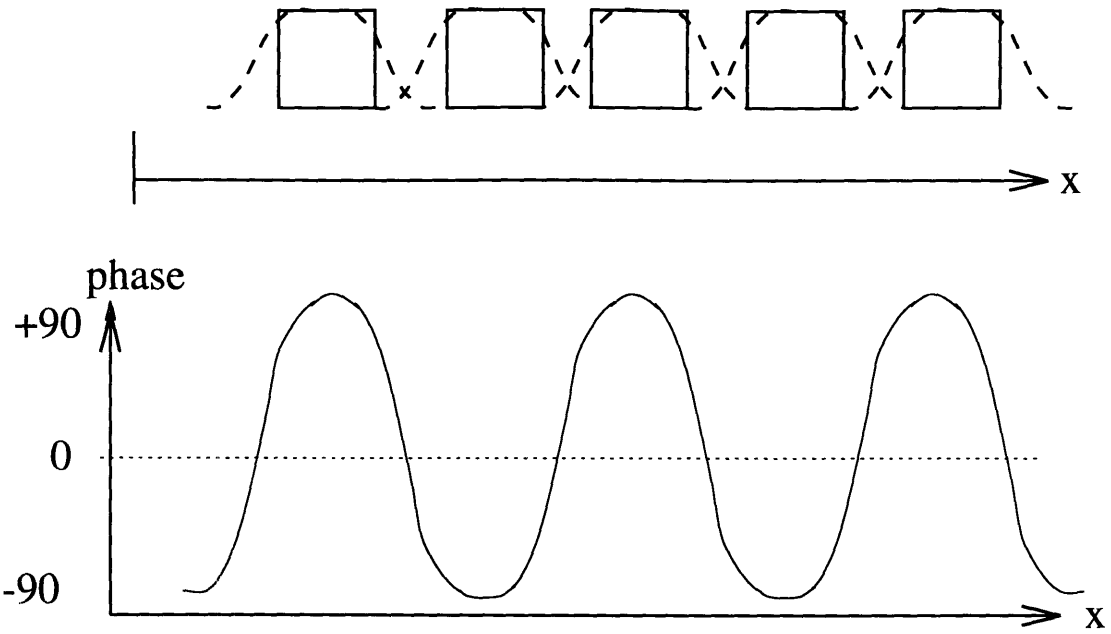

Figure 2-6: An Example of a Supermode

a scattering grating would be used to create this effect. This device was analyzed with the matrix array mode solver. The results showing the relative gain of the modes of the array are shown in Table 2.1 and the field profiles are shown in Figure 2-7. A BPM model using this gain profile, generated an electric field output showing lasing in the fundamental mode. The individual lasers were therefore locked in phase with each other, creating a coherent output beam.

2.3 Design Tolerance

2.3.1 Parallelism

There is concern that if the end-faces of the device are not exactly parallel, a coherent supermode would not be established within the laser array. This would be particularly true for a situation where deviation from exact parallelism is so great that the difference in the round trip distance at one end of the array is $\frac{\lambda}{2}$ greater than that at the other end.

For a lasing wavelength of $1.03\mu m$ in a device 500 microns wide, this would set the upper limit on deviation from parallelism (Δd max as shown in Figure 2-8 to be 0.0295° or 106.2 arc-seconds. Fortunately, the maximum parallelism error for devices fabricated at the Charles Stark Draper Laboratory is ± 3 arc-seconds. Parallelism of ± 0.1 arc-sec can be achieved with more precise equipment, though at substantially more cost per device.

To simulate the effect of 3 arc-seconds of deviation from parallel in the end-faces of the device, a short program was written in the C programming language which added a linearly increasing phase

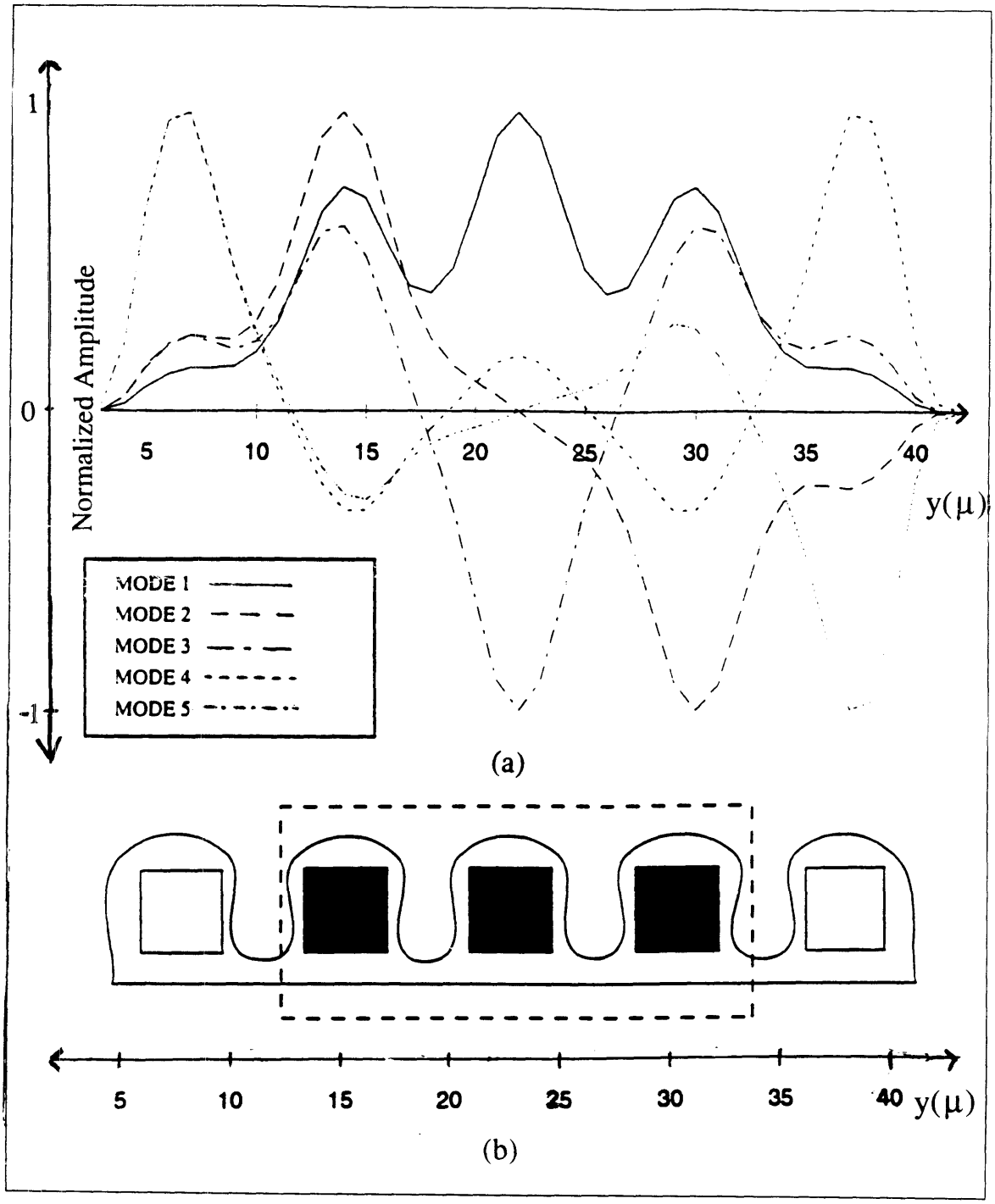

Figure 2-7: The Modes of a 5 Rib Laser Array

MODE	Neff(real)	Neff(imag.)	Gain($\frac{dB}{cm}$)
1	1.49253874	1.59E-05	8.21184798
2	1.49233425	1.31E-05	6.73006495
3	1.49199560	1.19E-05	6.10965197
4	1.49141523	4.47E-06	2.30325101
5	1.4912373	7.25E-06	3.73200289
6	1.49004531	1.14E-05	5.88208140

Table 2.1: The Relative Strengths of the Supermodes

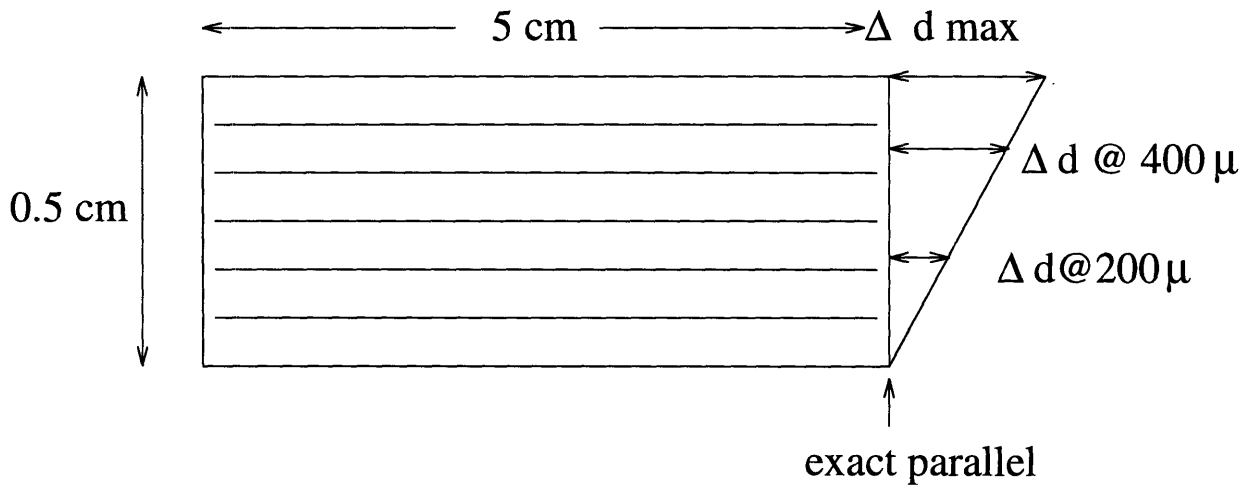

Figure 2-8: A Diagram of Deviations from Exact Parallelism

delay to the electric field at one end of the device. The delay represents the difference in phase caused by the light traveling the extra distance Δd to reflect off the non-parallel surface as shown in Figure 2-8

Our simulations show no difference in performance between a device with exactly parallel end faces and a device with the maximum deviation from parallelism of three arc-seconds.

2.3.2 Input Mode Tolerance

The inner cladding of the waveguide is highly multi-mode which causes nulls and others hot spots to occur in a time-varying pattern throughout the guide. The exact pattern of power distribution was considered too complex to model, therefore a uniform distribution of light was assumed. The lasers were also assumed to start lasing in a uniform distribution. These assumption caused concerns that the fundamental supermode dominated only because the assumed initial conditions favored the fundamental super-mode. A test was performed to determine the sensitivity of the fundamental supermode's dominance to adverse starting conditions. In this test, the array was assumed to begin lasing in a pattern nearly orthogonal to the fundamental supermode. A single wavelength sine wave, as shown in Figure 2-9, which closely resembles the first higher order supermode was used to describe the initial start-up pattern of the lasers. The results from the matrix array mode solver, found in Table 2.1 show that this mode is the higher order mode most likely to dominate over the fundamental mode. The test results showed that the fundamental mode dominated the array even in this worst start-up case, after only five round trip passes. This shows that the turn on condition does not affect the final modelocking of the array. It is assumed that if the fundamental mode can dominate over this extremely unfavorable start-up condition, fluctuations of the pump light distributions will not be able to cause another supermode to dominate. The section on results shows the simulation of the array with both the worst case sine wave initial lasing pattern and a slight deviation from parallelism.

2.4 Results

The BPM simulation using the worst case start-up conditions showed that the fundamental mode dominated the array quickly. The program generated field and phase plots of the electric field as it propagated down the waveguide in the x direction. These plots show that higher order modes initially dominated the array, but that the fundamental mode became dominant after the wave was exposed to the selected gain profile for nine reflections (45cm propagation) for the simulated values. Figure 2-10 shows a plot of the field intensity as the fundamental mode starts to dominate (the region x=30cm to x=45cm for the simulated values). The output of the BPM simulation is in color with violet representing the lowest intensity and red representing the highest intensity. On the black

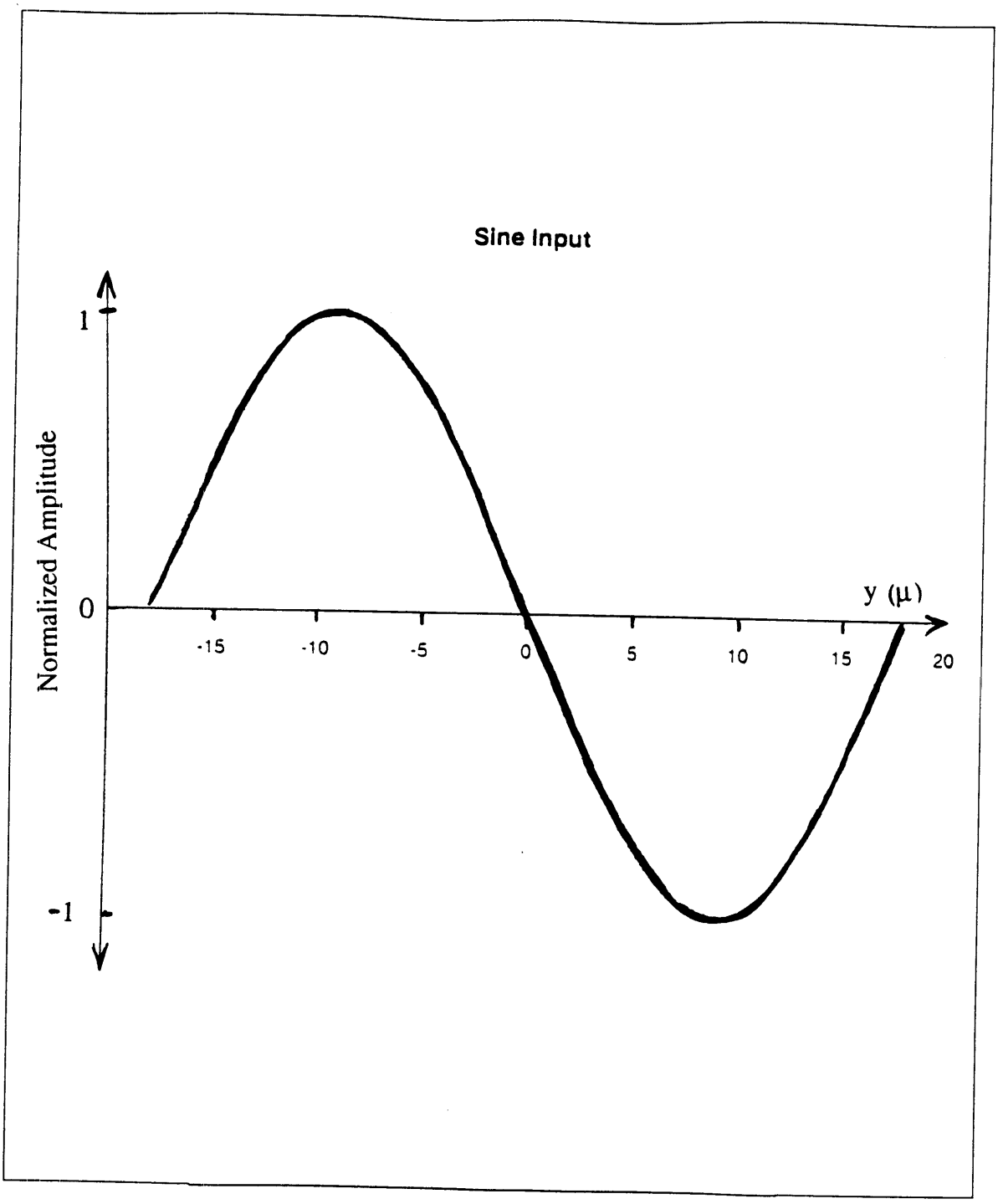

Figure 2-9: The Sine Wave Input Mode

and white reproduction shown here, the regions of various intensity are labeled with the appropriate color. The hot spots and nulls at the top of the plot show that the array is not phase-locked as it begins propagating in this region. However, in the middle of the propagation, the intensity becomes uniform across the array, indicate that the array is phase locked and the fundamental mode is dominant.

The phase plot in Figure 2-11 confirms these observations. The variations in light and dark in this plot indicate changes in phase with black representing $-90°$ and white indicating $+90°$. In this plot the broken horizontal lines represents in the top of the plot represents changes in phase across the waveguide, indicating that a higher mode is dominant. However, as the wave propagates in the x direction, the horizontal lines are less broken, indicating a more constant phase across the waveguide and the dominance of the fundamental mode. To show this more explicitly, a line graph was made of the phase across the waveguide after 40cm of wave propagation. It gives a more detailed view of the last horizontal bar shown in Figure 2-11. In this graph, shown in Figure 2-12, the vertical axis represents the phase rather than a color scheme. Figure 2-12 shows that the phase is constant across the array, with only slight edge effects.

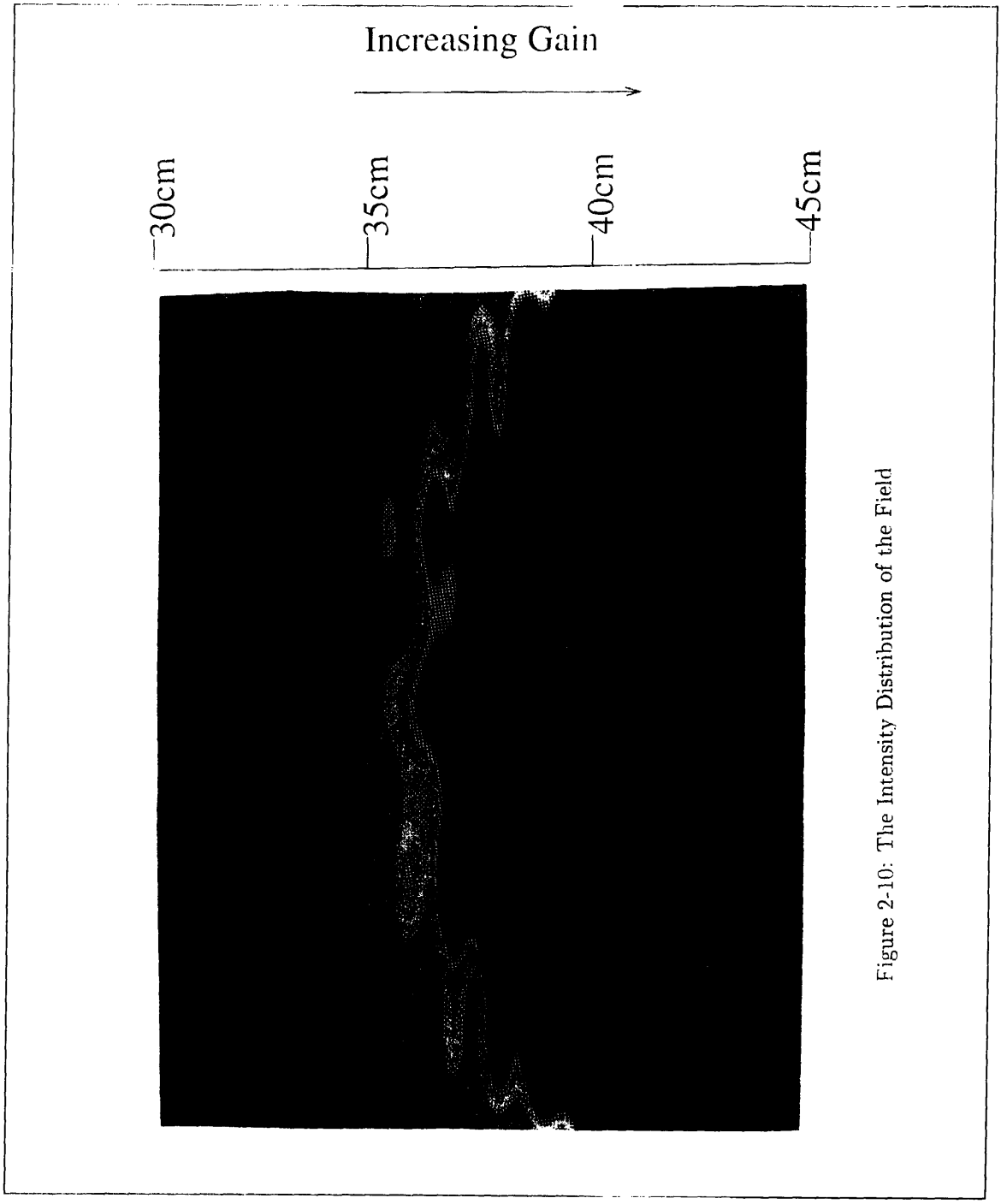

Figure 2-10: The Intensity Distribution of the Field

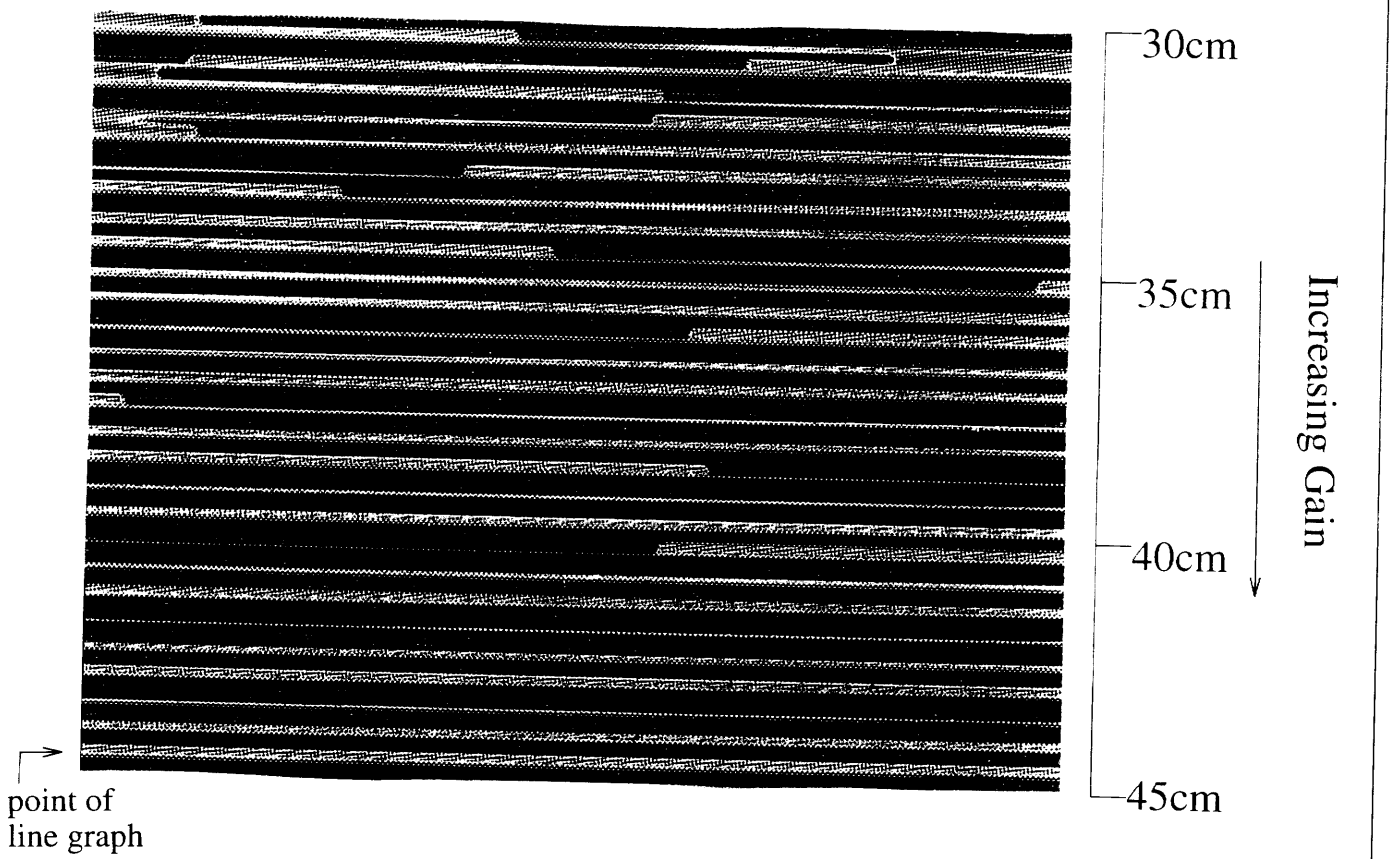

Figure 2-11: The Phase Distribution of the Field

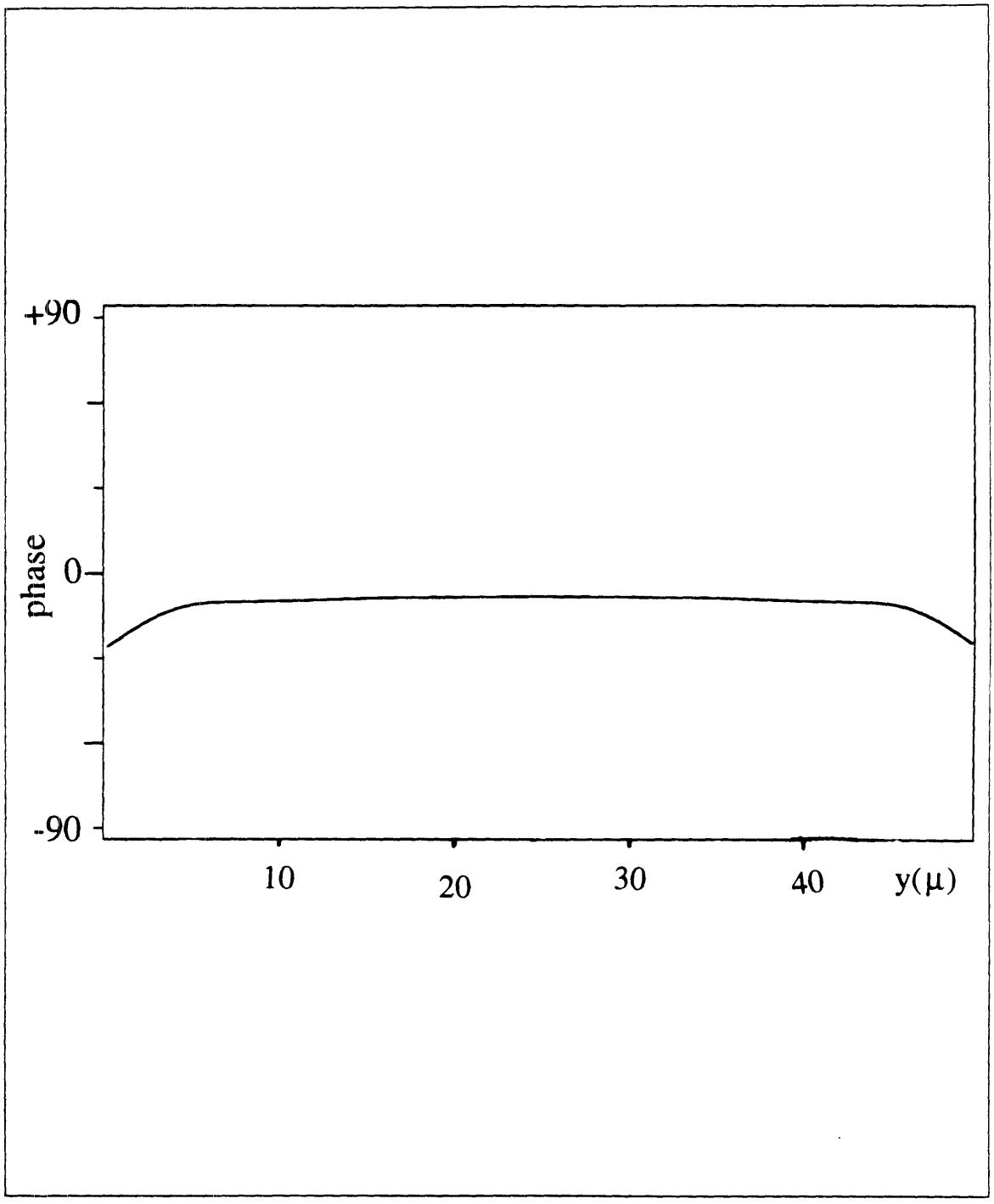

Figure 2-12: A Line Graph of the Phase at 20cm

Chapter 3

The Computer Simulation

3.1 The Beam Propagation Method

In this simulation, for the waveguide model in Figure 3-1, propagation in the horizontal direction (z-axis) and propagation in the vertical direction (y-axis) are considered independently. Propagation in the vertical direction is modeled using the effective index method discussed in section 3.4. However, propagation in the horizontal propagation, which determines the phase of the array, is solved directly using Maxwell's time-independent equations.

This simulation uses the Finite Difference Beam Propagation Method (FD-BPM or BPM) to solve Maxwell's equation in discrete space. In this simulation, the electric field is approximated as a scalar field at each of the computational steps as it propagates down the waveguide. A time-harmonic wave of the form:

$$E(x,t) = \mathbf{E}e^{-i\omega t} \tag{3.1}$$

is assumed. The propagation of the electro-magnetic wave through a non-homogeneous medium is governed by the Maxwell's equations:

$$\nabla \times E = -\frac{\delta B}{\delta t} = i\omega\mu_o H \tag{3.2}$$

$$\nabla \times H = \frac{\delta D}{\delta t} = -i\omega\epsilon_o n^2 E \tag{3.3}$$

$$\nabla \cdot (n^2 E) = 0 \tag{3.4}$$

$$\nabla \cdot H = 0 \tag{3.5}$$

Note that in these equations the time dependence of the electric and magnetic fields has been factored out. The resulting equations are then time-independent. The equation for the propagation of the

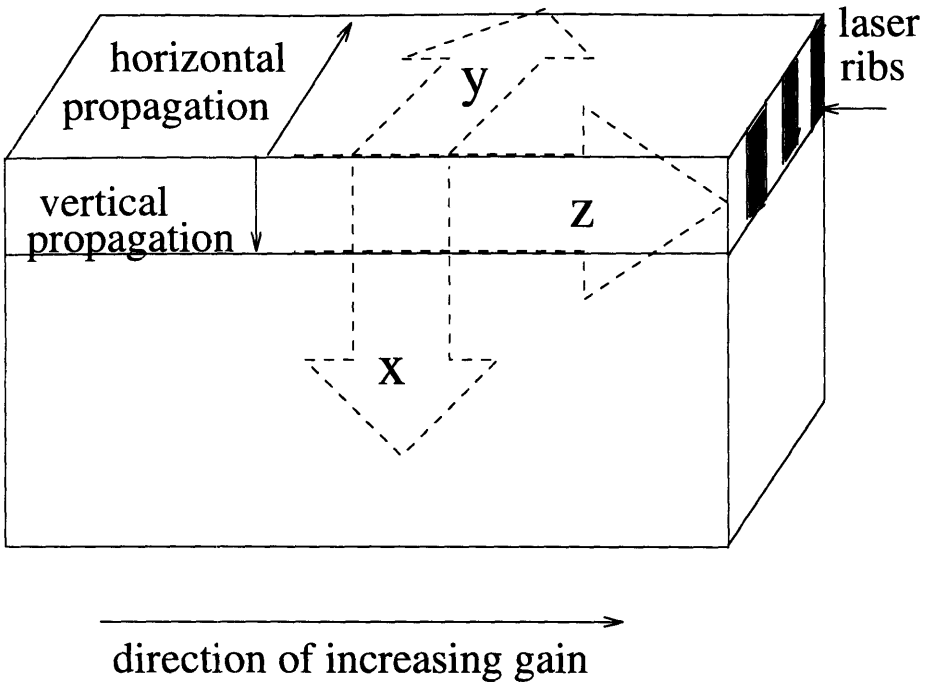

Figure 3-1: The Intensity Distribution of the Field

transverse-electric field is now derived. Taking the curl of the equation 3.2 yields:

$$\nabla \times (\nabla \times E) = \nabla \times (-\frac{\delta B}{\delta t}) = -\nabla \times (\mu \frac{\delta H}{\delta t}) \tag{3.6}$$

Using the identity:

$$\nabla \times (\nabla \times E) = \nabla(\nabla \cdot E) - \nabla^2 E \tag{3.7}$$

and assuming that polarization effects due to form birefringence and geometric polarization cross-talk are negligible; we assume

$$\nabla(\nabla \cdot E) = 0 \tag{3.8}$$

With this simplification equation 3.6 reduces to:

$$\nabla^2 E = \frac{\partial}{\partial t}(\nabla \times \mu H) \tag{3.9}$$

Substituting the equation 3.3 into equation 3.9 yields:

$$\nabla^2 \mathbf{E} = \mu \frac{\partial}{\partial t}(\frac{\partial \epsilon \mathbf{E}}{\partial t}) = \mu\epsilon \frac{\partial^2 \mathbf{E}}{\partial t^2} = -\mu\epsilon\omega^2 \mathbf{E} = -k^2 n^2 \mathbf{E} \tag{3.10}$$

where

$$\mathbf{E} = E e^{-ikn_a z} \tag{3.11}$$

where k is the wave number in free space ($k = \omega\sqrt{\mu_o \epsilon_o}$) and n_o is the reference index.

As the wave propagates in the z-direction, the field points in x and y are known at each step. Therefore, the second order derivative in t in the z-direction, which effects both the forward and backward propagation, is the only unknown. The. To solve for this, the ∇^2 operator is written in terms of its constituent parts:

$$\nabla^2 = \frac{\partial}{\partial x^2} + \frac{\partial}{\partial y^2} + \frac{\partial}{\partial z^2} \tag{3.12}$$

and the wave equation is expressed in terms of second derivatives:

$$-k^2 n^2 \mathbf{E} = \frac{\partial^2 \mathbf{E}}{\partial x^2} + \frac{\partial^2 \mathbf{E}}{\partial y^2} + \frac{\partial^2 \mathbf{E}}{\partial z^2}. \tag{3.13}$$

The derivatives $\frac{\partial^2 \mathbf{E}}{\partial x^2}$ and $\frac{\partial^2 \mathbf{E}}{\partial y^2}$ are known. The unknown second partial derivative in z is difficult to determine by computer methods for this model. However, simplifying assumptions can be applied to solve the problem. The second partial derivative in z can be fully expressed as:

$$\frac{\partial^2}{\partial z^2}(Ee^{-ikn_o z}) = [\frac{\partial^2 E}{\partial z^2} - 2ikn_o \frac{\partial E}{\partial z} - k^2 n_o^2 E]e^{-ikn_o z} \tag{3.14}$$

Assuming that the light is well contained by waveguide and that propagation closely parallel to the z axis, the paraxial approximation can be applied. This approximation assumes the field profile is slowly varying, therefore the second derivative in z can be set to zero reducing equation 3.14 to:

$$\frac{\partial^2}{\partial z^2}(Ee^{-ikn_o z}) = [-2ikn_o \frac{\partial E}{\partial z} - k^2 n_o^2 E]e^{-ikn_o z} \tag{3.15}$$

Substituting equation 3.15 back into the wave equation (3.13) yields:

$$-k^2 n^2 E = -i2kn_o \frac{\partial E}{\partial z} - k^2 n_o^2 E + \frac{\partial^2 E}{\partial y^2} + \frac{\partial^2 E}{\partial x^2} \tag{3.16}$$

Solving for the first derivative in z yields:

$$i\frac{\partial E}{\partial z} = \frac{\frac{\partial^2 E}{\partial x^2} + \frac{\partial^2 E}{\partial y^2} + k^2(n^2 - n_o^2)E}{2kn_o} = HE \tag{3.17}$$

This operation on the electric field E is represented by H, which is used in the computer program.

The equation 3.17 is a differential equation in continuous space. This can be approximated by difference equation in discrete space which can be solved by the computer. In discrete space, positions are represented as points on a three dimensional grid. A rough approximation of a derivative can be found by taking the difference between the value of the function at point x_i and x_{i+1} then dividing

by the distance between them as shown:

$$\frac{\partial f}{\partial x} \approx \frac{f(x_{i+1}) - f(x_i)}{\Delta x} \tag{3.18}$$

which is equivalent to the fundamental theorem of calculus when the limit is taken as delta goes to zero. Similarly, in discrete space, the approximation to the derivative becomes more accurate as the step size Δx becomes increasingly small.

There are three different ways to approximate derivatives with difference equations using variations of this method. These are known as the fully explicit, fully implicit and Crank-Nicholson solutions. The fully explicit solution uses the equation:

$$i\frac{E^{l+1} - E^l}{\Delta z} = HE^l \tag{3.19}$$

where E^{l+1} represents the field at point z_{l+1} and E^l represents the value of the field at point z_l. The value of the operator on E at the this step is determined by the derivative between the current step and the next. This method looks the least into the future to predict the next step. It is the least certain of the future behavior of the wave and is the most likely to make a wrong prediction which makes it unstable.

In the fully implicit solution:

$$i\frac{E^{l+1} - E^l}{\Delta z} = HE^{l+1} \tag{3.20}$$

The value of the operator on E at the next step is determined by the derivative between the current step and the next. This method looks the farthest into the future before predicting E^{l+1}. It is unconditionally stable, but numerically dissipative.

The Crank-Nicholson scheme is a compromise between these two methods. In this solution:

$$i\frac{E^{l+1} - E^l}{\Delta z} = \frac{HE^{l+1} + HE^l}{2} \tag{3.21}$$

The average of value of the operator on E at the this step and the value of the operator at the next step is determined by the derivative between the current step and the next. The Crank-Nicholson solution is both unconditionally stable and non-dissipative. It is also a difficult set of equations to solve. A system of linear equations in a matrix of the form $A \cdot x = B$ must be solved at every propagation step. For two dimensional problems, this matrix can be reduced to a tri-diagonal set of linear equations, which can easily be solved by a simple computer program. The Crank-Nicholson was chosen for the analysis of the waveguide because accuracy was more important that computational simplicity.

The BPM program solves the time-independent Maxwell's equations in discrete space. To solve the wave equation at the next propagation step the Crank-Nicholson scheme is used. A matrix

equation is solved at each propagation step and the field is simultaneously determined in x, y and z. Using this new field, the Crank-Nicholson finite difference equation is again solved and the process is repeated until the end of the specified propagation is reached.

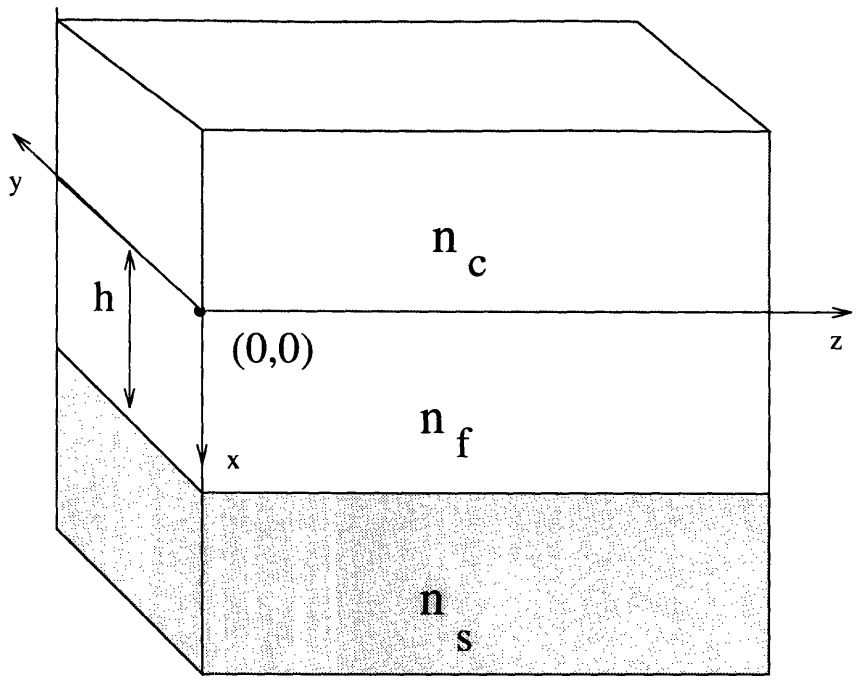

Figure 3-2: A Diagram of the Asymmetric Slab Waveguide

3.2 The Analytic Test

Analytic methods are the most reliable tool for analyzing an optical waveguide. For simple models this method is adequate, however as the complexity of the waveguide increases, analytic solutions become increasingly difficult to find. Computer models are then necessary for analysis. Unfortunately computer models such as those using the Beam-Propagation Method are subject to a number of errors. It is therefore necessary to compare the results of a computer generated model against a known analytic solution. The accuracy of the computational method can then be assessed and parameters of the computer code can be modified, if necessary, for greater accuracy or stability. This section describes how the analytic solution was found.

The equations used in the analytic method for an asymmetric planar slab waveguide have been previously derived [6]. The model for the waveguide is shown in Figure 3-2. In this model, n_f represents the higher indexed inner cladding, h represents the height of the inner cladding and n_c and n_s represent the cover and substrate layers, respectively. These layers are assumed to be infinitely large. The electro-magnetic power captured by the inner cladding will propagate in the z direction in the transverse electric (TE) mode as shown in Figure 3-3. The total velocity vector of the wave is nk. The κ component indicates the propagation velocity in the x-direction and β component indicates the propagation velocity in the z-direction. Vector addition yields the following equation

$$\kappa^2 = n^2k^2 - \beta^2 \tag{3.22}$$

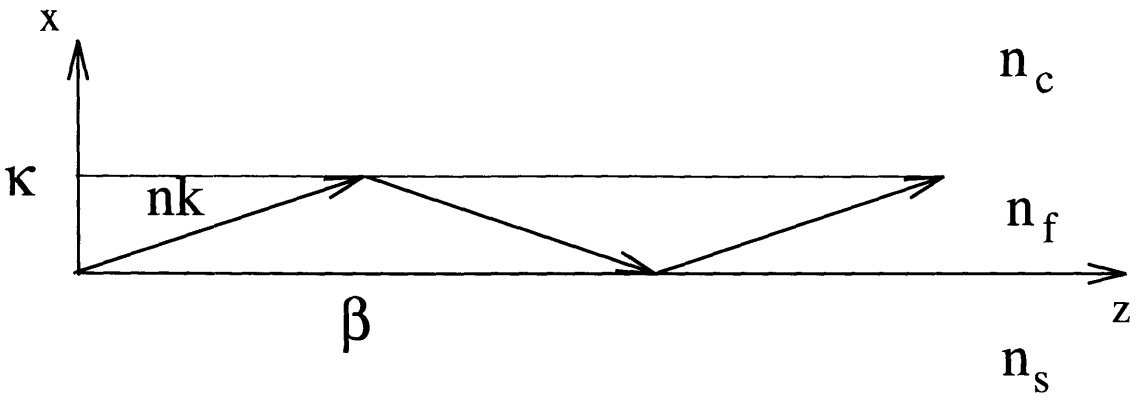

Figure 3-3: Determining the Wave Propagation Constant

In guided modes the film z-directed velocity then represents the propagation constant (β_f) and cover and substrate x-directed velocities represent the transverse decay constants (γ_c, γ_s) as defined by [6] the conditions for guidance will be discussed later:

$$\kappa_c^2 = n_c^2 k^2 - \beta^2 = -\gamma_c^2 \tag{3.23}$$

$$\kappa_f^2 = n_f^2 k^2 - \beta^2 \tag{3.24}$$

$$\kappa_s^2 = n_s^2 k^2 - \beta^2 = -\gamma_s^2 \tag{3.25}$$

Where the subscripts c, f, and s refer to the cover, film and substrate respectively. To determine the conditions for guidance, the equations for propagation are solved with the appropriate bounding conditions. The TE modes in a planar waveguide are governed by the the following equations:

$$H_y = E_x = E_z = 0 \tag{3.26}$$

$$H_x = -\frac{\beta}{\omega\mu} E_y \tag{3.27}$$

$$H_z = \frac{-i}{\omega\mu} \frac{\partial E_y}{\partial x} \tag{3.28}$$

For the E_y component of the wave traveling in the x-direction, we write the field in terms of the x-directed velocity, κ:

$$E_y = E_o e^{i\kappa x} \tag{3.29}$$

and take the second derivative, substituting in for κ^2 according to Equation 3.22:

$$\frac{\partial^2 E_y}{\partial x^2} = -\kappa^2 E_y = (\beta^2 - n^2 k^2) E_y \tag{3.30}$$

The following solutions to this equation are assumed for the cover, film, and substrate regions, respectively [6]:

$E_y = E_c \exp(-\gamma_c(x-h))$ for $h < x$ (cover)

$E_y = E_f \cos(\kappa_f x - \phi_s)$ for $0 < x < h$ (film)

$E_y = E_s \exp(\gamma_s x)$ for $x < 0$ (substrate)

Boundary condition are applied to solve for ϕ_s. These conditions demand that E_y and $\frac{\partial E_y}{\partial x}$ be continuous across the film boundaries at x=0 and x=h. Applying these to the film-substrate boundary yields [6]:

$$E_s = E_f \cos(-\phi_s) \tag{3.31}$$

$$-\gamma_s E_s = E_f \kappa_f \sin(-\phi_s) \tag{3.32}$$

Dividing the second equation by the first yields:

$$-\gamma_s = \kappa_f \tan(-\phi_s) \tag{3.33}$$

Therefore:

$$\phi_s = \arctan(\frac{\gamma_s}{\kappa_f}) \tag{3.34}$$

Now that ϕ_s is known, the constants can be determined. The equations can be normalized by setting E_f to one. E_s and E_c can then be found by evaluating E_s at x=0 and E_c at x=h:

$$E_c = \cos(\kappa_f h - \phi_s) \tag{3.35}$$

$$E_s = \cos(-\phi_s) \tag{3.36}$$

To solve for the field distribution from these equations, it is now only necessary to evaluate β and set n_f,n_c and n_s. The choice of indices which would allow propagation of only the fundamental was determined by using the dispersion relation [6]:

$$\kappa_f(\beta)h - \phi_s(\beta) - \phi_c(\beta) = \nu\pi \tag{3.37}$$

This condition states that in one round trip for a film of thickness h, the total phase from the propagation, $\kappa_f 2h$ plus the phase shifts induced by the boundaries, $2(-\phi s)$ at the substrate and $2(-\phi_c)$ at the cover must equal an integer multiple of 2π. This integer number represented by ν is called the mode number. This condition is always valid. To determine if a mode guided, the guidance equation is solved transcendentally for β. From Equation 3.30 it can be shown that the

wave is guided (κ_c, κ_s are imaginary) only when:

$$kn_f > \beta > kn_c \tag{3.38}$$

and

$$kn_f > \beta > kn_s \tag{3.39}$$

For every guided mode, κ_f is real, κ_s and κ_c are imaginary and there exists an integer ν for which the dispersion relation holds. To determine if the model of the slab was single mode, equation 3.37 was solved for $\nu = 1$. If β could not be found by Mathematica^{TM}'s root-finding algorithm, it was determined that the first order mode could not propagate and that the slab model was single mode. Using Mathematica, it was determined from experimentation that for h=2μ, and $\kappa_0 = 7.76 \times 10^6 (\lambda = .807\mu)$, the indices $n_c = n_s = 1.45$ with $n_f = 1.455$, $n_f = 1.460$ and $n_f = 1.465$ respectively would generate single mode slabs. The transverse electric field distributions for these slabs were then calculated and these analytic results were compared to results from a BPM computer simulation of the same models. The results are shown in Section 3.3.

3.3 Correspondence of the Results

The simple slab waveguides described in section 3.2 with h=2μ, were both simulated and analyzed using a wavelength of $\lambda = .807\mu$, an index of 1.45 for the cover and substrate and indices of 1.455, 1.460 and 1.465 respectively for the film. The BPM program simulated the electric field output from these models and the results were exported to an EXCEL^{TM} spreadsheet. To compare these results to the analytic solutions, the electric field equations from section 3.2 were solved for discrete values of x over the range of zero to twenty-five microns at intervals of 0.5μ using an EXCEL speadsheet. An EXCEL plotting feature allowed the analytic and computer generated results to be plotted on the same axes. These plots are shown in Figures 3-4, 3-5 and 3-6. These graphs show almost perfect correspondence. This shows that the BPM program generates accurate results and that these results are not index specific.

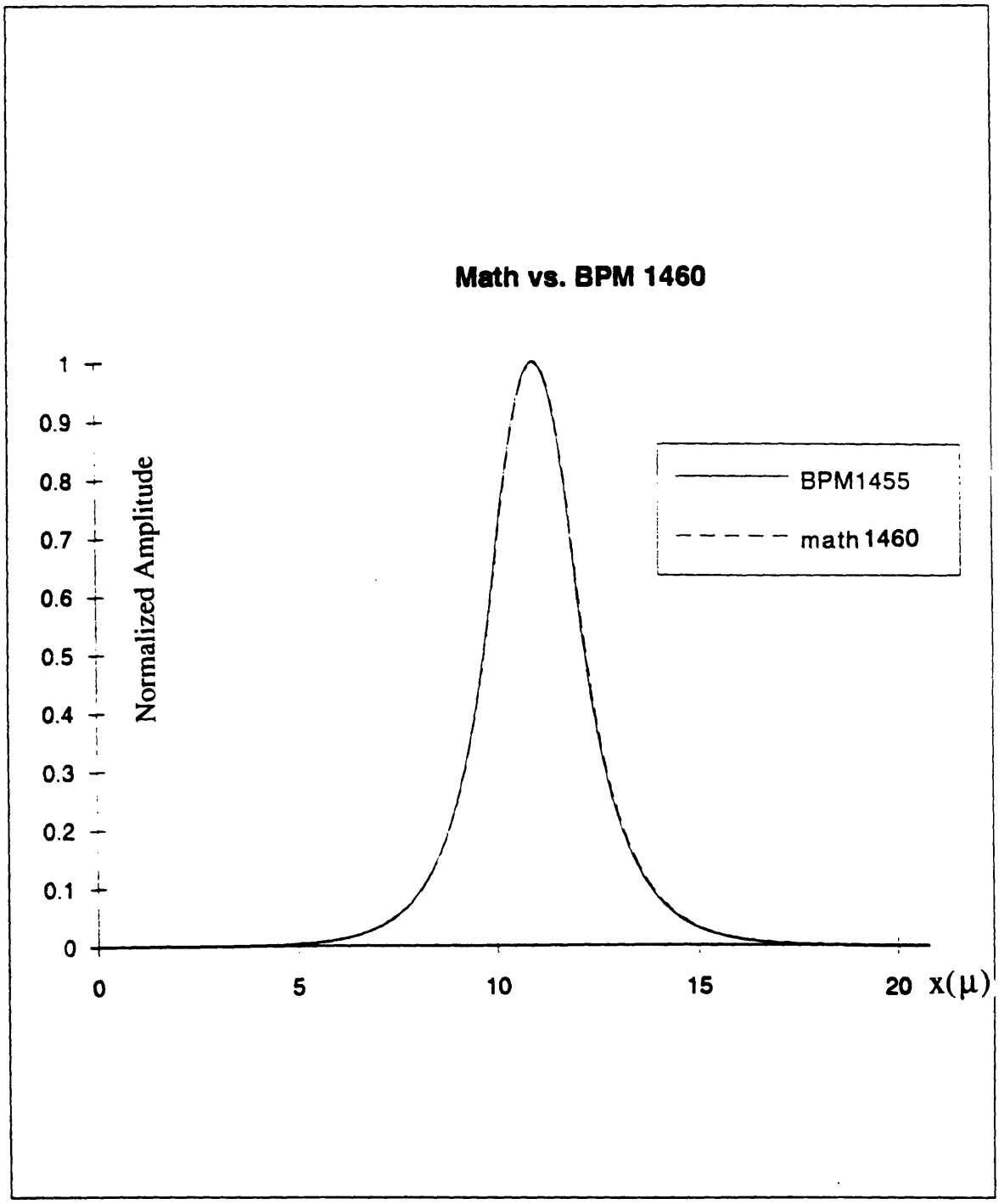

Figure 3-4: BPM and Analytic Results for Film Index 1.460

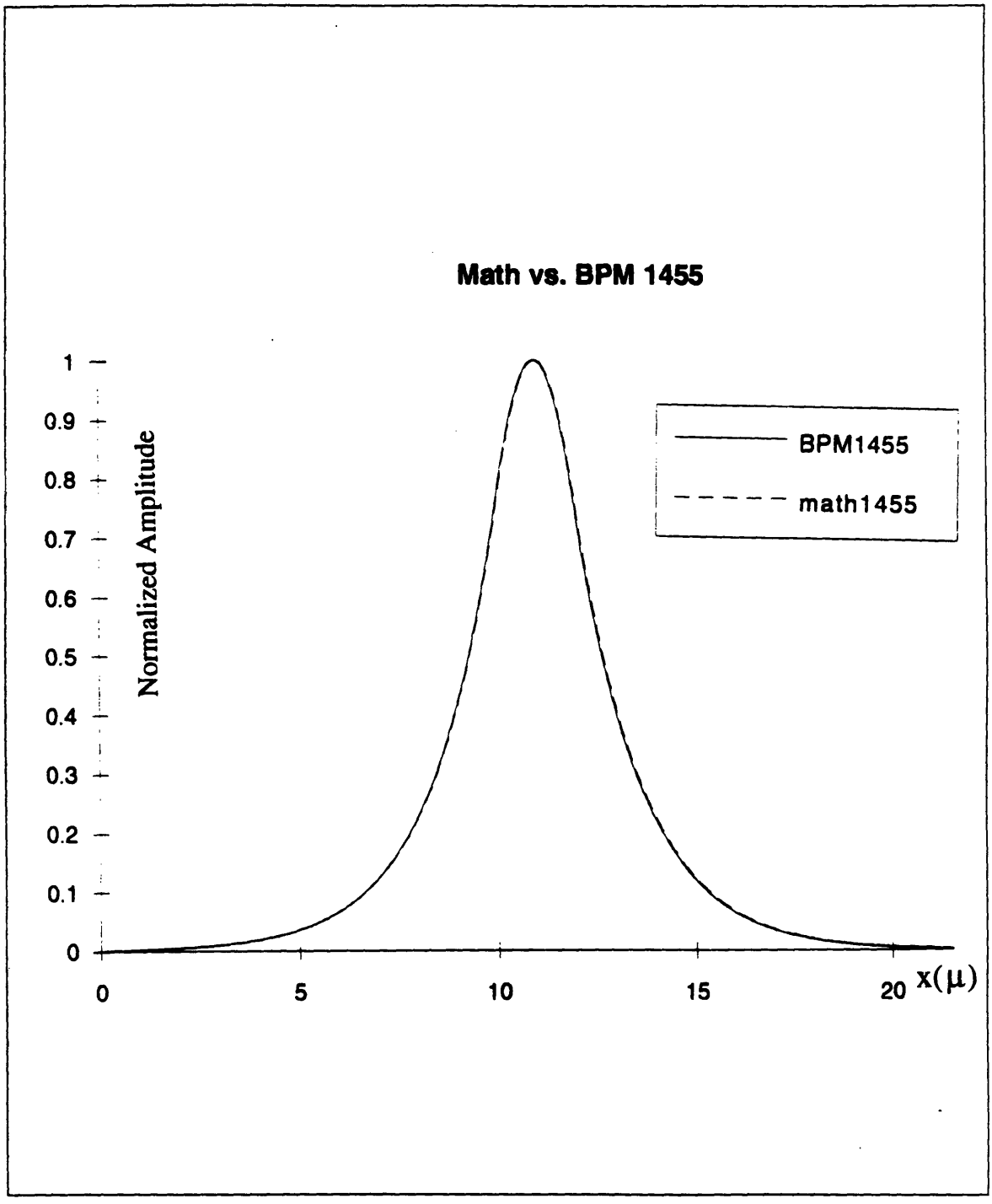

Figure 3-5: BPM and Analytic Results for Film Index 1.455

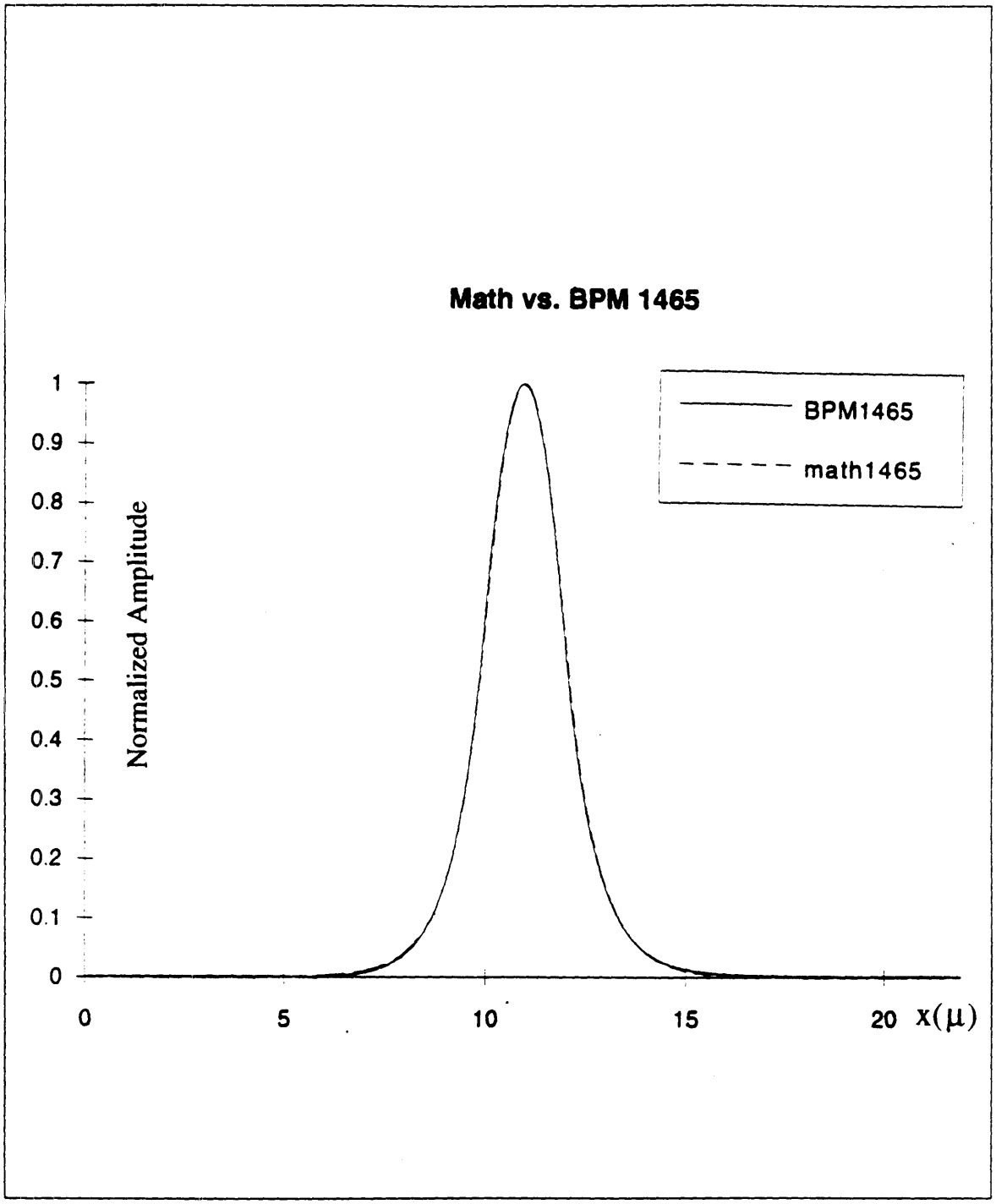

Figure 3-6: BPM and Analytic Results for Film Index 1.465

3.4 The Matrix Array Mode-solver

Although the BPM program is accurate, it was very computationally intensive. Therefore, a matrix array mode solving program was used to quickly determine a doping profile which would favor the fundamental mode. The program was based on a mode solving method developed by L.M. Walpita [7]. The matrix array program uses a simple algorithm and determines the effective index for each of the modes of the laser array. The mode with the largest imaginary index experiences the greatest gain and dominates the laser array. When a profile which favored the fundamental mode was found, a model with this profile was created and simulated with the BPM program. The BPM simulation confirmed that this doping profile would cause the array to lase in the fundamental mode.

The matrix array program solves the imaginary index of the supermodes in two steps. First, the structure is divided into sections as indicated by the dashed lines in Figure 3-7 (a). Each section is modeled as a TE polarized multi-layer stack, as shown in Figure 3-7 (b) and its effective index is determined. This effective index in the vertical direction (as determined by Figure 3-1) is used for both the matrix simulation and the BPM simulation. The entire array is then modeled as a TM polarized multi-layer stack using these effective indices as shown in Figure 3-7 (c). The effective index for each of the modes in array (c) is then determined by the mode solver. These effective indices will determine the relative strengths of the supermodes of the laser array structure.

To solve for the effective index of a multi-layer stack, the matrix array mode solver uses Maxwell's equations and boundary conditions. The boundaries and directions of propagation are shown in Figure 3-8. Horizontal propagation corresponds to propagation in the y direction across the guide. In this direction, the array is modeled as the two dimensional multi-layer stack as shown in Figure 3-9.

Solving Maxwell's equations for the TM guided modes of the waveguide in Figure 3-8 is similar to the solution for the TE modes of the asymmetric slab waveguide in section 3.2. The equations which govern wave propagation for the array in Figure 3-9 are:

$$H_{jx} = -A_{j1}\exp[-p_{jy}(y - y_{j-2}) + B_j]\exp[p_{jy}(y - y_{j-2})] \tag{3.40}$$

$$i\omega n_j^2 \epsilon_o E_{jz} = -p_{jy}A_{j1}\exp[p_{jy}(y - y_{j-2})] + p_{jy}B_j\exp[p_{jy}(y - y_{j-2})] \tag{3.41}$$

where the y-directed and z-directed propagation constants p_y and p_z are related to κ and β in Section 3.2 by:

$$p_y = i\beta \tag{3.42}$$

$$p_z = (\beta^2 - k^2 n^2)^{\frac{1}{2}} = \kappa \tag{3.43}$$

and A_j and B_j are the forward- and backward-propagation wave amplitudes, j represents the layer

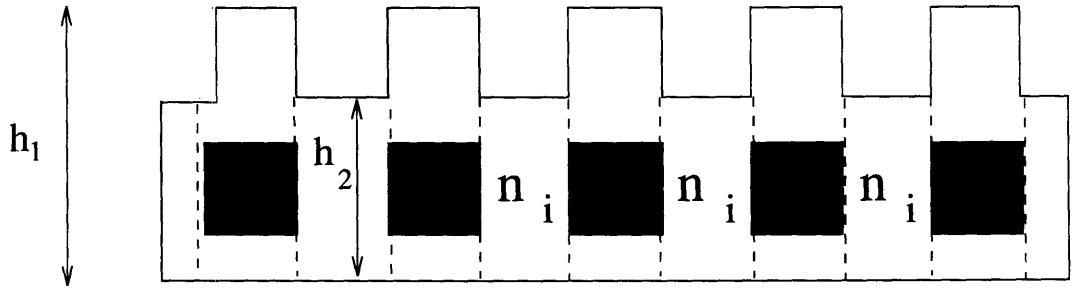

(a) Physical array with gain in ribs

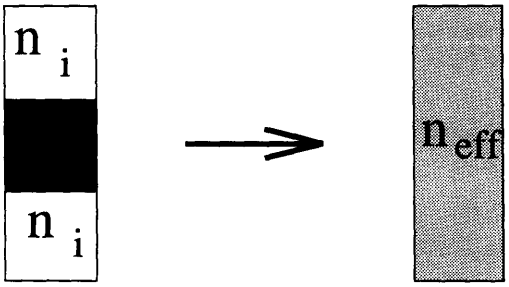

(b) Each section modelled with an effective index $(n_r > n_{eff} > n_i)$

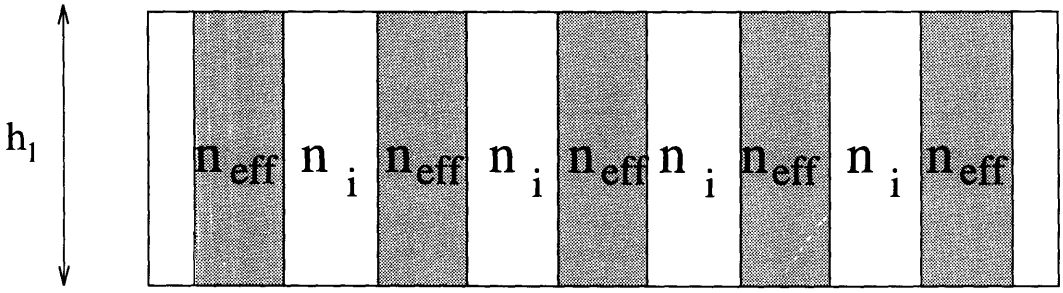

(c) Array represented as a multi-layer stack using effective indices

Figure 3-7: Propagation in the Multi-Layer Stack

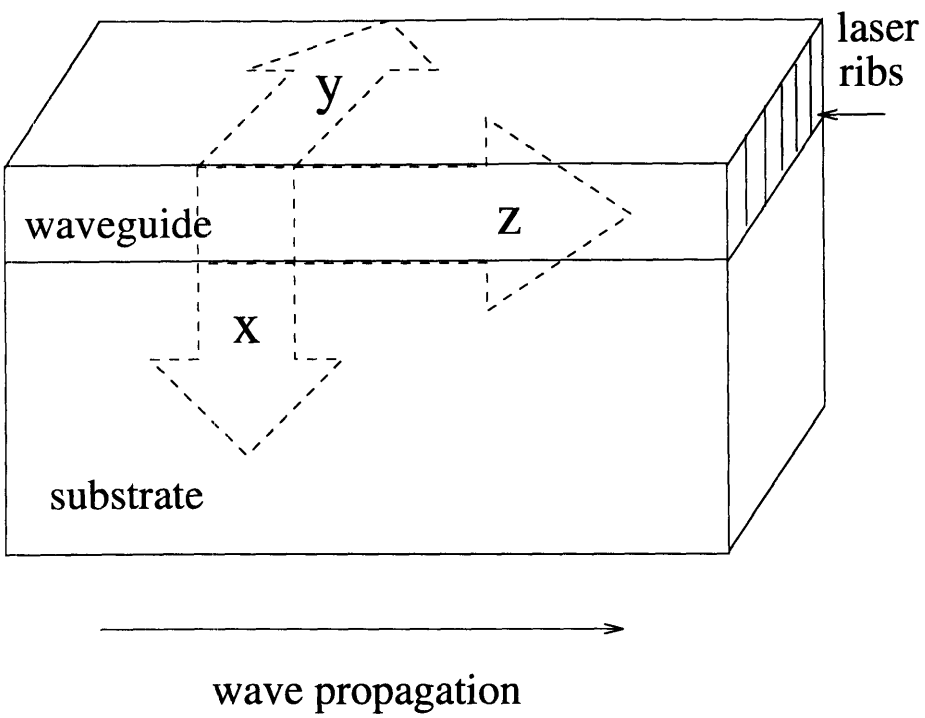

Figure 3-8: Direction of Propagation in the Matrix Model

numbers, x, y, z represent the vector direction and ϵ_0 is the free-space permittivity.

Assuming no charge build-up in the waveguide, the boundary conditions that tangential electric fields and perpendicular magnetic fields must be continuous across the boundaries allows the electric fields at the j^{th} layer to be equated to the $(j-1)^{th}$ and $(j+1)^{th}$ layer at the boundaries. Therefore, equations 3.40 and 3.41 for the $(j-1)^{th}$ and $(j+1)^{th}$ layers can be related to each other with the transfer matrix M_j [7]. The transfer matrices for each of the layers can then be multiplied together to create a single transfer for the entire structure. Therefore, the field amplitude of the first layer can be related to the field amplitude of the n^{th} layer by the equation:

$$\begin{vmatrix} A_n \\ B_n \end{vmatrix} = \begin{vmatrix} M_n & M_{n-1} & M_{n-2} & ..... & M_3 & M_2 & M_1 \end{vmatrix} \begin{vmatrix} A_1 \\ B_1 \end{vmatrix} = \begin{vmatrix} M_T \end{vmatrix} \begin{vmatrix} A_1 \\ B_1 \end{vmatrix} \tag{3.44}$$

where M_T is a single four by four matrix which can be written as:

$$\begin{vmatrix} M_T \end{vmatrix} = \begin{vmatrix} \alpha_1 & \alpha_2 \\ \alpha_3 & \alpha_4 \end{vmatrix} \tag{3.45}$$

The energy of the waveguide is trapped within the region y=0 and $y = y_{n-2}$. The field outside of this region is evanescent. Therefore, there should be no forward propagating wave in the substrate and no backward propagating plane wave in the superstrate. To satisfy this condition, B_n and A_1

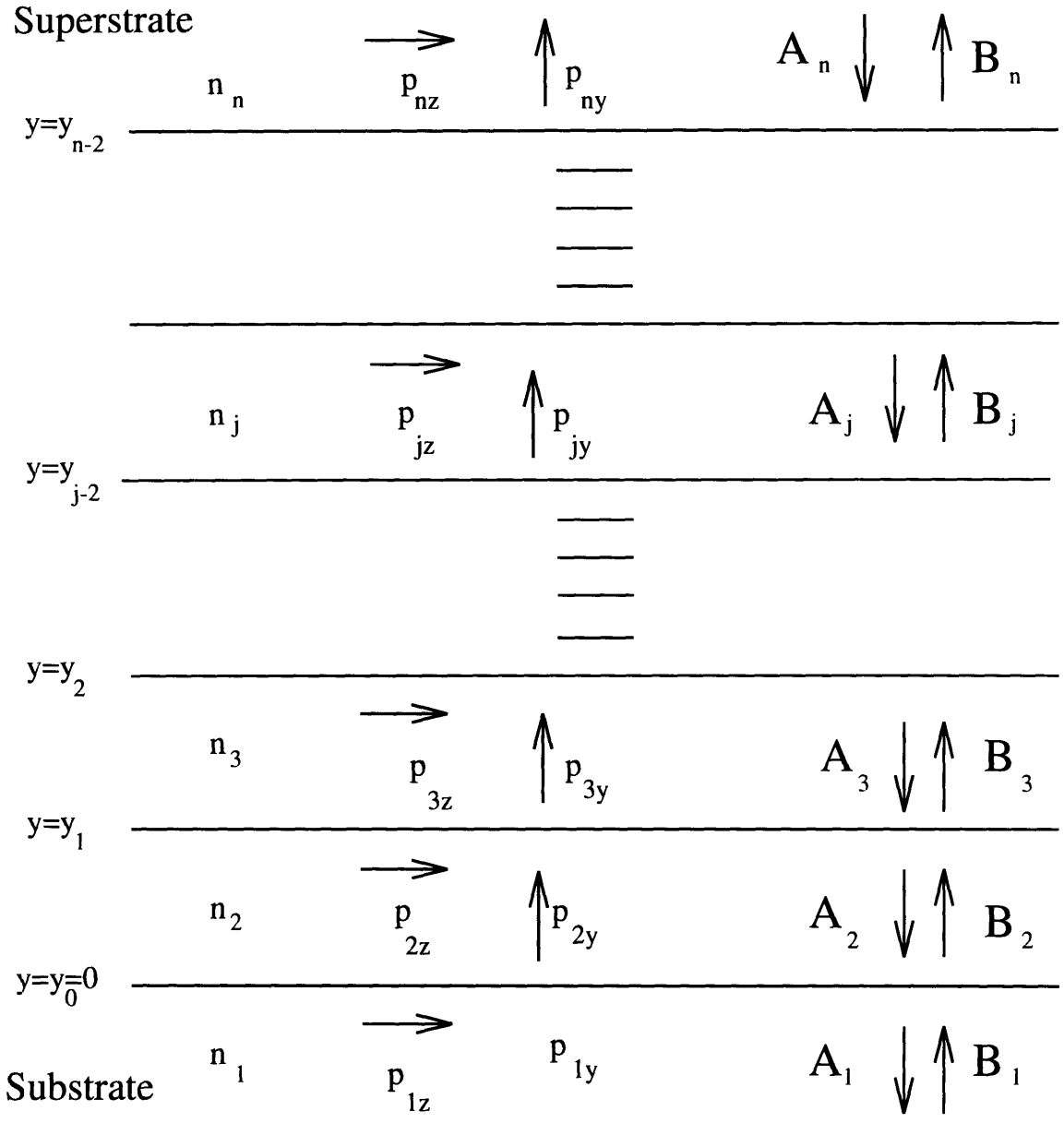

Figure 3-9: Propagation in the Multi-Layer Stack

in equation 3.45 will be zero as shown:

$$\begin{vmatrix} A_n \\ 0 \end{vmatrix} = \begin{vmatrix} \alpha_1 & \alpha_2 \\ \alpha_3 & \alpha_4 \end{vmatrix} \begin{vmatrix} 0 \\ B_1 \end{vmatrix} \tag{3.46}$$

This matrix equation can be satisfied only if the element α_4 of the matrix is equal to zero. α_4 is a function of $\frac{\beta}{k}$, the normalized propagation constant in the x-direction. Because the physical index characteristics of the guide are known, the equation $\alpha_4 = 0$ can be solved for β for each of the supermodes of the array [7]. The effective index is then determined from this propagation constant.

Chapter 4

Conclusions

The waveguide designed and modeled in this thesis is an excellent method of utilizing the power of semi-conductor laser diode arrays in a coherent output beam. The design is sturdy and immune to the spatial mode of the pump source. If mass produced, it could replace HeNe lasers in laser printers and be used in other applications where small coherent laser systems are needed

With further modification, this device could be doped with erbium and pumped entirely by the side pumping method as shown in Figure 4-1. This would create an excellent compact amplifier for inter-continental fiber-optic cables.

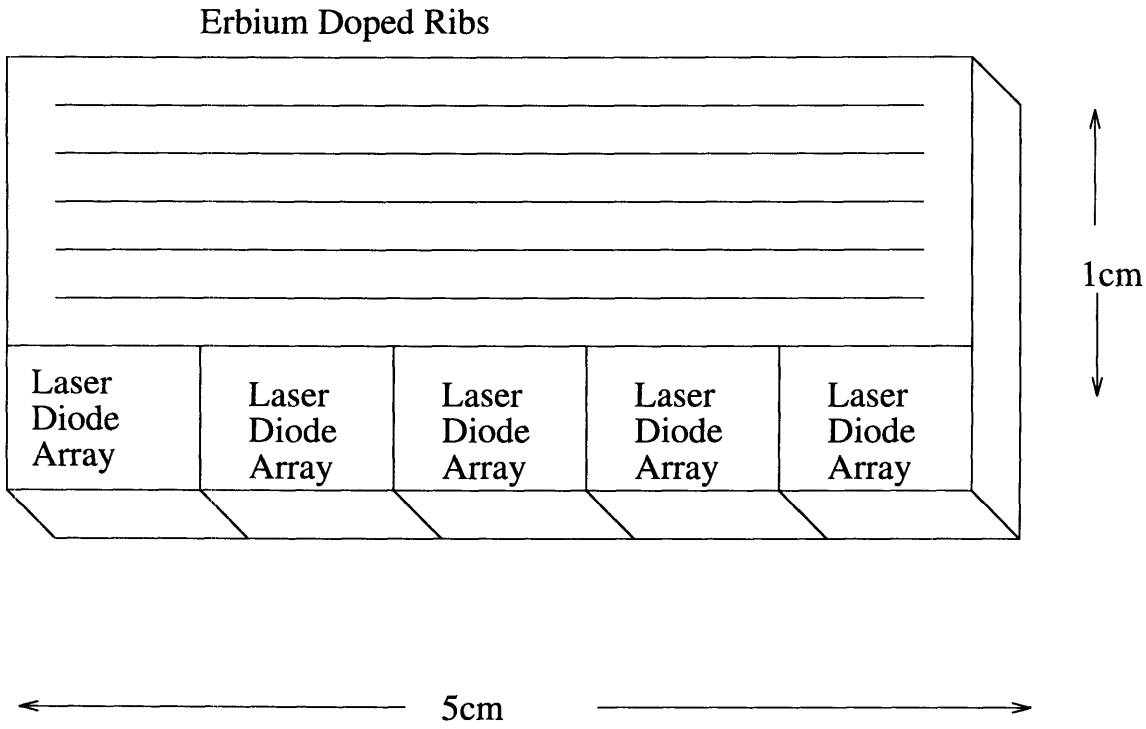

Figure 4-1: A Possible Compact Fiber Amplifier at 1.55μm

Bibliography

[1] Lily Xee Pang. *Ultrashort Optical Pulse Generation From High Power Diode Arrays.* PhD thesis, Massachusetts Institute of Technology, March 1993.

[2] L. Goldberg and J. F. Weller. Injection locked operation of a 20 element coupled-stripe laser array. *Electronic Letters*, 50:1713, 1987.

[3] J. E. Epler and G.S. Jackson et. al. Mode-locked coupled stripe quantum well laser operation in a tunable external cavity. *Applied Physics Letters*, 47:1022, 1985.

[4] M. Segev, Y. Ophir, and B. Fisher. Mode locking and frequency tuning of a laser diode array in an extended cavity with a photorefractive phase conjugate mirror. *Applied Physics Letters*, 57:2523, 1990.

[5] H. Masuda and A. Takada. Picosecond optical pulse generation from a mode locked phased laser diode array. *Electronic Letters*, 25:1418, 1989.

[6] E. Tamir. *Topics in Applied Physics vol. 7:Integrated Optics.* Springer-Verlag, 1975.

[7] L. M. Walpita. Solutions for planar optical waveguide equations by selecting zero elements in a characteristic matrix. *Journal of the Optical Society of America:A*, 2:595–601, 1985.